Comments on Inorganic Chemistry
Publication details, including instructions for authors and subscription information:
http://www.informaworld.com/smpp/title~content=t713455155

Analysis, Design and Engineering of Simple Iron-Sulfur Proteins: Tales from Rubredoxin and Desulforedoxin

José J. G. Moura[a]; Brian J. Goodfellow[a]; Maria J. Romão[ab]; Frank Rusnak[ac]; Isabel Moura[a]
[a] Departamento de Química (and Centro de Química Fina e Biotecnologia), Faculdade de Ciências e Tecnologia, Universidade Nova de Lisboa, Portugal [b] Apartado 127, 2780 Oeiras, Portugal and IST, Departamento de Química, Instituto de Tecnologia Química e Biológica, Lisboa, Codex [c] Department Biochemistry and Molecular Biology, Mayo Clinic Foundation, Rochester, MN, USA

To cite this Article Moura, José J. G. , Goodfellow, Brian J. , Romão, Maria J. , Rusnak, Frank and Moura, Isabel(1996) 'Analysis, Design and Engineering of Simple Iron-Sulfur Proteins: Tales from Rubredoxin and Desulforedoxin', Comments on Inorganic Chemistry, 19: 1, 47 — 66
To link to this Article: DOI: 10.1080/02603599608032727
URL: http://dx.doi.org/10.1080/02603599608032727

Analysis, Design and Engineering of Simple Iron–Sulfur Proteins: Tales from Rubredoxin and Desulforedoxin

JOSÉ J. G. MOURA, BRIAN J. GOODFELLOW, MARIA J. ROMÃO*, FRANK RUSNAK** and ISABEL MOURA
Departamento de Química (and Centro de Química Fina e Biotecnologia), Faculdade de Ciências e Tecnologia, Universidade Nova de Lisboa, 2825 Monte de Caparica, Portugal.

Received March 15, 1996; accepted April 15, 1996

The most thoroughly characterized non-heme iron center in biology is Rubredoxin, the simplest member of the iron–sulfur class of metalloproteins. Rubredoxin contains a high-spin iron atom with tetrahedral coordination by four cysteinyl sulfur atoms. A structural variant of this center is found in Desulforedoxin, the smallest known Rubredoxin type protein. The 3D structure of both Rd and Dx has been determined at high resolution. These two proteins can therefore be used as case studies in which structural control by the polypeptide chain over the metal site can be discussed in detail.

INTRODUCTION

Anaerobic sulfate reducing bacteria (SRB) contain a wealth of metalloproteins that have brought to light many novel metal centers and unusual

**Instituto de Tecnologia Química e Biológica, Apartado 127, 2780 Oeiras, Portugal and IST, Departamento de Química, 1096 Lisboa Codex. ***Department Biochemistry and Molecular Biology, Mayo Clinic Foundation, Rochester, MN 55905, USA.*

Comments Inorg. Chem.
1996, Vol. 19, No. 1, pp. 47–66
Reprints available directly from the publisher
Photocopying permitted by license only

combinations of metal sites.[1] One of the simplest iron-containing proteins isolated from SRB is Rubredoxin (Rd). Desulforedoxin (Dx), isolated from the sulfate reducing bacterium *Desulfovibrio (D.) gigas*, is also a small protein (homo-dimer with 36 amino acids per subunit), containing a high-spin iron atom bound by four cysteinyl residues, a metal center similar to that found in Rd type proteins.[2] The protein lacks histidine, arginine, proline, isoleucine, phenylalanine, and tryptophan. Each monomer of Dx has one iron atom bound to four cysteinyl residues.[3–5] The metal binding motif in Rd consists of two pairs of cysteinyl sulfur ligands with two amino acids separating cysteines of each pair (Fig. 1). The amino acid sequence of the polypeptide chain of Dx has a distinctive feature: an unusual sequence of cysteine residues. Contrary to the Rd type centers, the Dx sequence places the two final cysteines in consecutive positions.[6] These adjacent cysteines (Cys 28 and 29) impose distortions on the ideal tetrahedral coordination that are reflected in the spectroscopic properties of the protein. The problem has wider implications since Dx and Rd centers appear as distinct domains in association with other types of centers (see below).

The structural arrangement of the iron and the four cysteinyl ligands in Dx has been extensively probed by complementary spectroscopic methods, and its X-ray structure has been solved at 0.18 nm resolution.[5–7]

This article is organized in order to discuss:

(i) the methods that were used to probe the ligands of the active site of Dx (spectroscopic data including: electronic spectra, electron paramagnetic resonance (EPR) and Mössbauer (MB)),
(ii) the 3D structure of Dx, which is compared with the other known $Fe–S_4$ protein, Rd (2D NMR and X-ray data),
(iii) the structural features of the metal site with detailed information on angles and distances at the metal site, and
(iv) how the properties of the site are modulated by the polypeptide chain.

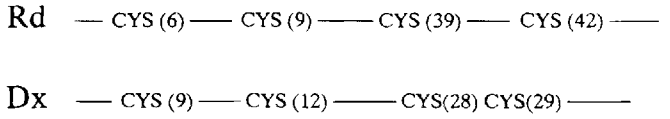

FIGURE 1 Schematic comparison of Rubredoxin and Desulforedoxin amino acid sequences giving relevance to the cysteine residue distribution.

Site-directed mutagenesis and mimetic chemistry exemplify how it is possible not only to reveal the structural contraints around the metal and which ligands bind to the metal, but also to modulate specific structural features and, in essence, design novel structures with desirable (bio)chemical properties.

SPECTROSCOPIC DATA

Electronic Spectra

For simple Fe–S proteins, charge-transfer bands are characteristic of the Fe site geometry and indicate the subtle differences and similarities between Dx and Rd. In Fig. 2, a comparison of the electronic spectra of Rd and Dx is presented (Dx has one aromatic residue while Rd has six). Dx shows absorption maxima at 507, 370 and 278 nm. The maxima for the visible spectrum of Dx are shifted and the characteristic Rd shoulder at 350 nm is not observed. The extinction coefficient for Dx is 4,580 $M^{-1}cm^{-1}$ (per monomer) at 507 nm, similar to values observed for other Fe–S proteins.[3]

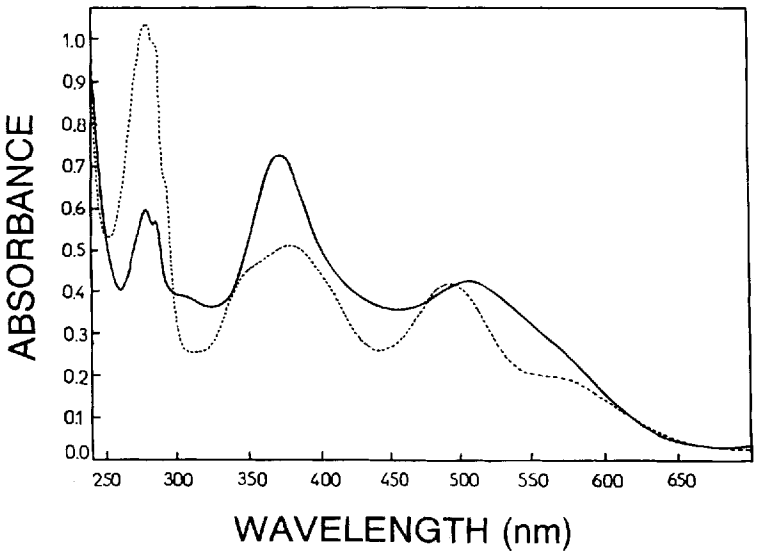

FIGURE 2 Comparison of the electronic spectral features (ultra-violet and visible regions) of Rubredoxin (---) and Desulforedoxin (——).

Metal Substitution

Different metals are readily introduced into Rd type centers via reconstitution of the apoprotein with appropriate metal salts.[5] Rd and Dx derivatives containing Ni and Co have been analyzed by UV/vis, NMR, EPR and MCD.[8–10] ^{57}Fe replacement has been used for MB studies, and an indium derivative was used to solve the 3D X-ray structure of Dx. Substitution of the native iron in Rd by ^{113}Cd, ^{199}Hg and Zn has been carried out and the protein studied by NMR. In particular, the diamagnetic Zn derivatives of Dx and Rd have been fully explored by 2D NMR spectroscopy (Refs. 11–13, see below).

Renewed interest in Ni-substituted Rds has emerged due to the structural features revealed by the crystallographic studies of [NiFe] hydrogenases, indicating that the Ni active site (in interaction with a heavy scatterer, probably iron) is coordinated to four cysteinyl residues.[14] Rd and Dx substituted with Ni have been shown to mimic the hydrogenase activity.[15]

Electron Paramagnetic Resonance Studies

To understand the EPR (and MB) properties of Dx, some background theory is necessary.

The magnetic properties of half-integer spin systems ($S > 1/2$) can be described by the following spin Hamiltonian:

$$\hat{H}_e = D\left[\hat{S}_z^2 - 1/3\ S(S+1) + E/D\left(\hat{S}_x^2 - \hat{S}_y^2\right)\right] + g_0\beta\,\hat{S}.\hat{B} \qquad (1)$$

for which D and E are parameters describing the zero-field splitting of the spin multiplet. It is assumed that the Zeeman interaction is isotropic ($g_0 \sim 2$) and the energy levels are calculated under conditions for which the zero-field splitting is larger than the energy involved in the EPR transition ($D \gg g_0\beta B$), a condition valid for Rd and Dx. Under these conditions each Kramers doublet can be treated separately, assuming a fictitious spin, $S' = 1/2$. The properties of each doublet can be described by a term $S'\cdot g'\cdot\hat{B}$ where the principal g'-values of the g'-tensor depend only on the parameter E/D. The g' values can be computed directly from Eq. (1), and the variation of the g'-values of the Kramers doublets as function of E/D has been described.[16] Analysis of this diagram is useful for interpreting the EPR data of systems with $S = 5/2$ but with different E/D values.

In its oxidized form, Rd contains one high-spin ferric atom (magnetic moment $\mu = 5.73$ Bohr magnetons). The EPR spectrum is highly con-

served for Rds isolated from different species. The EPR resonances for Rd can be interpreted as arising from transitions within the ground and first excited doublet state (middle Kramers doublet) of the high-spin ferric center ($S = 5/2$) with a high degree of rhombic distortion ($E/D = 0.28$) (Fig. 3-A).[16] As the temperature is lowered, the $g' = 4.3$ signal decreases in intensity, while the middle Kramers doublet becomes thermally depopulated, and the $g' = 9.4$ resonance originating from the ground state increases.

In contrast, the Dx EPR spectrum reveals a high-spin ferric state with nearly axial symmetry ($E/D = 0.08$) (Fig. 3-B).[4,5] The principal g'-features are observed at 7.7 and 5.7 and broad components at 4.1 and 1.8. The observed g'-values calculated for a high-spin ferric ion, associated with the three Kramers doublets for an $E/D = 0.08$, are shown in Fig. 3-C. The resonances at 4.1, 7.7 and 1.8 are attributed to the ground state doublet ($\pm 1/2$) and the resonance at $g' = 5.7$ to the middle doublet ($\pm 3/2$). When the temperature is decreased, the signal at $g' = 7.7$ increases while the signal at $g' = 5.7$ decreases. The zero-field splitting was estimated to be 2 cm^{-1}.[5]

At low salt concentrations a surprising result is observed in the EPR spectrum of oxidized Dx:[5] the EPR signal quantifies only up to ca. 0.5 spins/1Fe. Increasing the ionic strength increases the number of spins quantified by EPR to ca. 1 spin/1Fe. In addition, MB studies revealed that at low ionic strength there are fast relaxing centers that can not be seen by changing the environment of the EPR-active spins (so that they become detectable by EPR). This is caused by the increase in ionic strength which changes the relaxation properties of the center. This problem may be the origin of low EPR quantitations observed in other cases.

Mössbauer Studies

In order to evaluate a Mössbauer spectrum, the Hamiltonian of Eq. (1) has to be augmented by terms describing the hyperfine interactions with the ^{57}Fe nucleus:

$$\hat{H}_{hf} = A_0 . \mathbf{S}.\mathbf{I} - g_n \beta_n \mathbf{B}.\mathbf{I} + eQV_{xx}/12\left(3I_z^2 - 15/4 + \eta\left(I_x^2 - I_y^2\right)\right), \quad (2)$$

and the spectrum can be simulated by the spin Hamiltonian:

$$\hat{H} = \hat{H}_e + \hat{H}_{hf} \quad (3)$$

using the parameters listed in Table I.

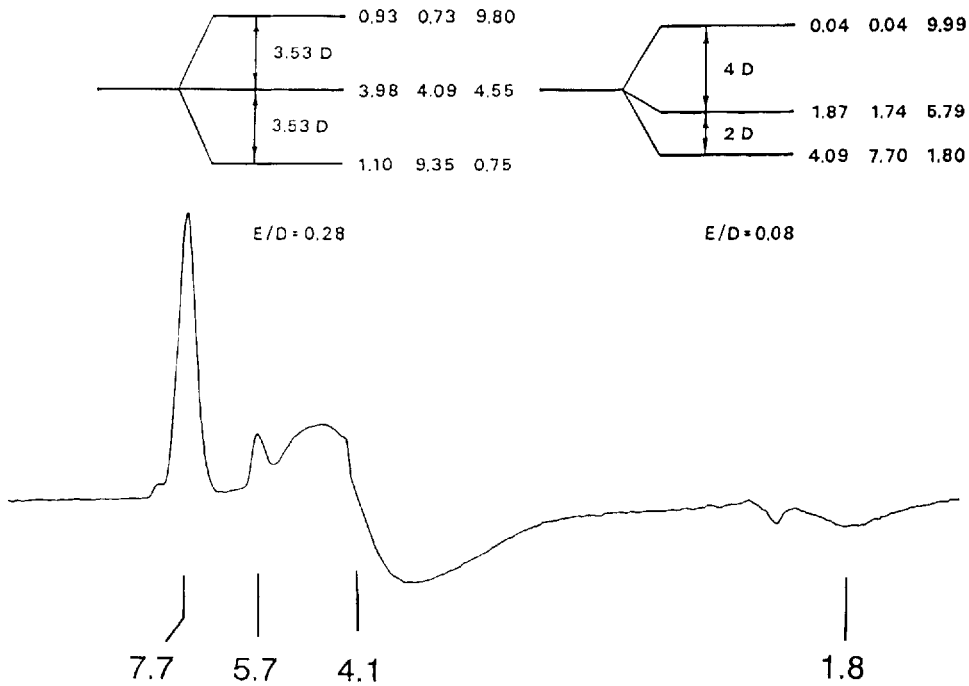

FIGURE 3 X-band EPR spectrum of Desulforedoxin at 5 K. In the top of the spectrum, a schematic representation of the energy levels of a $S = 5/2$ spin multiplet for $E/D = 0.28$ (Rd) and $E/D = 0.08$ (Dx) and respective g'-values of each Kramers doublet is indicated.

TABLE I

Selected spin Hamiltonian parameters for oxidized and reduced Desulforedoxin.

	Oxidized Desulforedoxin	Reduced Desulforedoxin
D (cm^{-1})	+2.2	−6
E/D	0.080	0.19
g_x	2.0	2.08
g_y	2.0	2.02
g_z	2.0	2.20
$A_x/g_n\beta_n$ (kG)	−154	−200
$A_y/g_n\beta_n$ (kG)	−154	−200
$A_z/g_n\beta_n$ (kG)	−154	−67
ΔE_Q (mm/s)	−0.75	+3.55
δ (mm/s)	+0.25	+0.70
β (degrees)	90	10

Isomeric shifts are quoted relative to iron metal at room temperature.

At 4.2 K, at high salt concentration and in the presence of a weak field (0.6 kG), the Mössbauer data of Dx indicate that 80% of the spin population is in the ±1/2 doublet.

For samples with low salt concentrations at low temperatures, a quadrupole doublet with $\Delta E_Q = 0.75$ mm/s in addition to the magnetic spectrum (the doublet sometimes represented up to 50% of total iron) was observed. The isomeric shift, $\delta = 0.25$ mm/s, was the same as that seen for the magnetic spectrum, indicating that the doublet results from a Dx-type chromophore.

In order to obtain a good estimation of the D value, Dx was studied in different applied magnetic fields. After numerous simulations, a value for $D = 2.2 \pm 0.3$ cm^{-1} was obtained, which is in good agreement with the EPR measurements.[5]

The spin Hamiltonian parameters shown in Table I demonstrate that the saturation field and the isomer shift of Dx are characteristic of a tetrahedral sulfur environment. Unlike Rd, the zero-field parameter E/D of Dx is small, indicating different environments at the two metal sites.

The MB parameters for reduced Dx are $\Delta E_Q = 3.55$ mm/s and $\delta = 0.70$ mm/s. The isomer shift is typical for high-spin ferrous ions with tetrahedral sulfur coordination. By recording the MB spectrum of reduced Dx at 200 K in a field of 5.5 T, it can be proven that $\Delta E_Q > 0$, while for Rd, $\Delta E_Q < 0$. This observation suggests that the ground state orbital of reduced Dx is of predominantly $d_{x^2-y^2}$ character, while reduced Rd is a

pure d_{z^2} orbital.[5] From spectra of the reduced form of Dx at 4.2 K and at different magnetic fields, the zero field splitting parameters ($D = -6$ cm^{-1} and $E/D = 0.19$) were obtained.

TOTAL CHEMICAL SYNTHESIS OF DESULFOREDOXIN

Due to the simplicity of the polypeptide chain and the iron center, Dx was chemically synthesized via solid phase peptide synthetic methods. A 36 amino acid polypeptide chain was synthesized based on the known amino acid sequence of native Dx. The iron site was then reconstituted and the biochemical and spectroscopic characteristics investigated. The final product has an identical sequence to the protein isolated from *D. gigas*. The synthetic and natural Dx are very similar in terms of redox potential and spectroscopic properties (electronic spectra, EPR and MB).[17]

OVER-EXPRESSION AND CONVERSION OF DESULFOREDOXIN INTO A RUBREDOXIN CENTER

The gene encoding Dx has been cloned from *D. gigas* genomic DNA using the polymerase chain reaction, expressed in *E. coli* and purified to homogeneity.[18] The physical and spectroscopic properties of the recombinant protein resemble those observed for the native protein isolated from *D. gigas*. These include an α_2 tertiary structure, the presence of bound iron, and absorbance maxima at 370 and 506 nm in the electronic spectrum due to ligand to iron charge transfer bands. Low temperature EPR studies confirm the presence of a high-spin ferric ion with an *E/D* value close to the native protein. Interestingly, *E. coli* produced two forms of Dx containing iron. In addition to the dimer form containing iron, a second form containing equimolar amounts of zinc and iron was also obtained.

The spectroscopic properties of Dx are believed to result from a distortion of the metal site due to the presence of adjacent cysteine residues in the metal binding motif. In order to address the structural basis for this distortion, two mutants of Dx have been generated in which either a Gly residue or Pro-Val residues have been inserted between these neighboring cysteines.[19] The optical and EPR properties

of the ferric complexes of both mutants are distinct from the wild type protein and are virtually identical to Rd. The low temperature X-band EPR spectrum of each mutant was characteristic of high-spin Fe^{3+}; each exhibits a large rhombic distortion (E/D = 0.21–0.23). Interestingly the ferric complexes of both mutants are unstable, indicating that additional features in the wild type protein contribute to the stability of the iron–sulfur center.

3D STRUCTURE OF DESULFOREDOXIN

Crystallographic Analysis

The X-ray structure of Rd was solved early in 1981,[2] while those of Dx(Fe^{3+}) and of an indium derivative (see Metal Substitution section) were reported in 1995.[7] For Dx, the crystals diffracted beyond 0.18 nm, which allows comparisons with the high resolution structure for Rd. A ribbon representation of the Dx dimeric structure is shown in Fig. 4 (color plate at the end of this article). The Dx molecule is a homodimer consisting of two subunits of 36 amino acids each, with overall approximate dimensions of 24 Å × 24 Å × 22 Å. Each monomer consists of an antiparallel β-sheet extending from Asp5 to Val18. Two turns are present at the metal binding site, Cys9–Gln14 and Cys28–Glu31. This antiparallel β-sheet extends upon dimer formation, resulting in a four-stranded sheet connected by interchain hydrogen bonds. These four-stranded antiparallel β-sheets have a large twist between the first and forth strands. Parallel to these four strands is a short section of interchain β-sheet (Val27 chain A-Val27 chain B). The C-termini also adopt β-sheet conformations with interactions occurring between Gln36 and Val6.

The iron center is located near the surface of the molecule. It is bound to the four cysteine residues Cys9–X–X–Cys12 and Cys28–Cys29 as expected, with no other ligands in close proximity to the metal. A diagram of the iron site and data on the distances of the Fe–S bonds for the $Fe–S_4$ center is shown in Fig. 5. The corresponding values for the Rd center are also displayed. For Dx, while all four Fe–S bond lengths are practically equivalent, the Sγ–Fe–Sγ angles range from 102° to 119°. Coordination of the iron to both vicinal cysteines, Cys28 and Cys29, brings about an enlargement of the Sγ–Fe–Sγ angle relative to an exact tetrahedral geometry. The deviations from ideal tetrahedral geometry of the Sγ–Fe–Sγ angles for Dx and Rd are shown in Fig. 6.

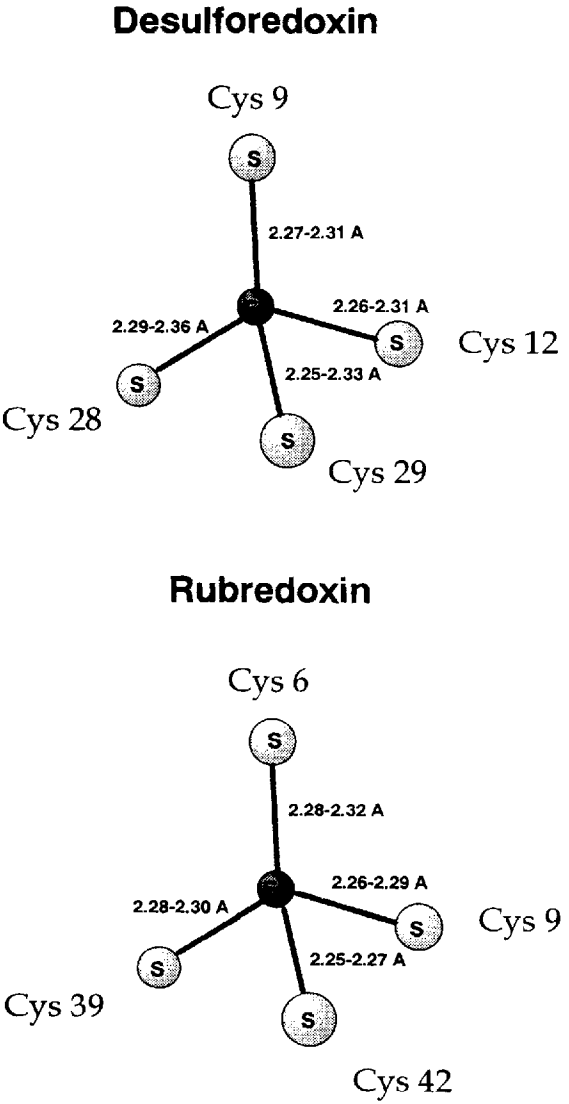

FIGURE 5 Schematic representation of the metal site geometries for Dx and Rd. Values given correspond to ranges of values for subunit A and B of Dx and to ranges of values for different Rds isolated from *Desulfovibrio* sp.

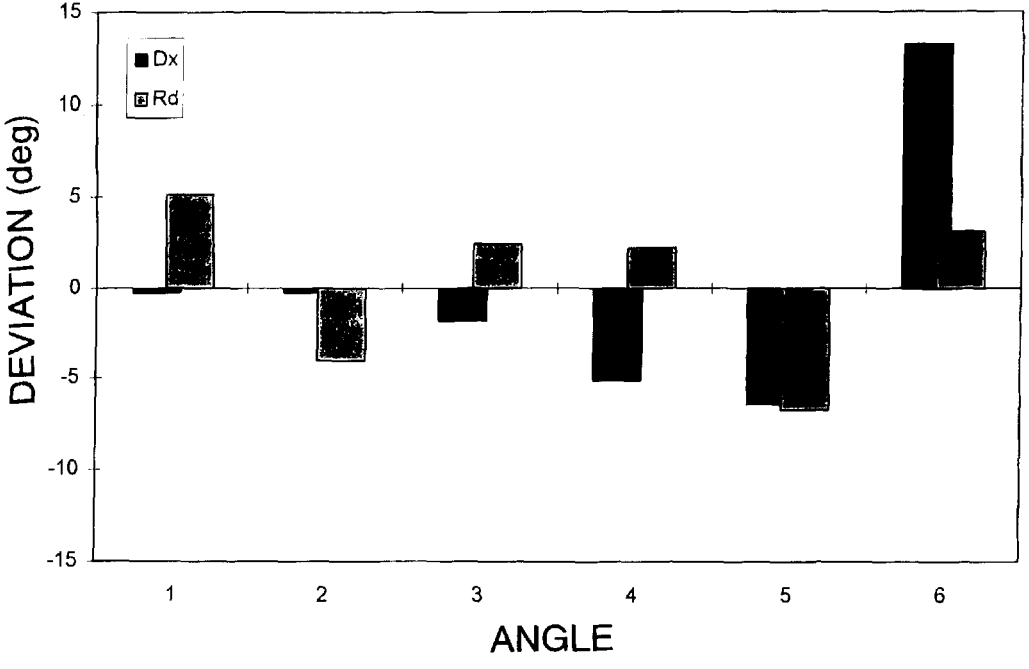

FIGURE 6 Deviation from ideal tetrahedral angles for the Fe–S_4 centers in Desulforedoxin and Rubredoxin. Angles are labeled as: (**1**) Cys9(6)–Cys12(9); (**2**) Cys9(6)–Cys29(42), (**3**) Cys9(6)–Cys28(39); (**4**) Cys12(9)–Cys29(42), (**5**) Cys12(9)–Cys28(39) and (**6**) Cys28(39)–Cys29(42). Numbers in parentheses refer to Rubredoxin.

The study of Fe–S proteins by NMR was first carried out in the early 1970's and has since been an area of extensive investigation. Work done with Fe–S proteins has also been used as a base from which the fundamentals of NMR and paramagnetic proteins have arisen.

The use of NMR for structural determination of macromolecules is a well-developed technique. The structure and dynamics of macromolecules can be investigated in solution and the method is complementary to X-ray. However, there are a number of limitations, the most important for Fe–S proteins being the relaxation properties of the metal center. In some Fe–S proteins the metal center contains unpaired electrons which cause nearby protons to relax very rapidly, resulting in the loss of these signals in the NMR spectrum due to line broadening. The metal center can also produce large chemical shift changes for nearby protons when compared to a diamagnetic analogue. These factors can be problematic when standard NMR experiments are employed. Even so, a number of structural NMR studies of paramagnetic Fe–S proteins have been carried out.[20] Recently a number of 3D structures of Fe–S proteins have been determined solely by NMR methods. Standard 2D NMR methods were used along with 1D selective NOE experiments to obtain assignments for hyperfine shifted resonances.[21–24]

A relatively easy way to overcome the bleaching problem of paramagnetic centers is to replace the metal with a diamagnetic equivalent (although it should be noted that this is not always possible). A number of studies of Rd with replacement of the Fe by ^{113}Cd, ^{199}Hg and Zn have been carried out. Standard 2D NMR methods were used and structures obtained.[11,12] No major differences between the global folding of the NMR and X-ray derived structures were detected.

The 1D spectrum of Dx(Fe^{3+}) indicates that the high spin d^5 arrangement of the ferric site ($S = 5/2$) causes severe line broadening.[13] The Fe^{3+} center can be reduced, however, with dithionite to give the Fe^{2+} species. This ferrous form ($S = 2$) shows much narrower lines as a result of the reduced paramagnetism. Some resonances, however, are shifted well outside the normal diamagnetic region (100–300 ppm). These are assumed to be due to cysteinyl β-CH_2 protons shifted due to their close proximity to the iron unpaired electrons.[25,26]

For structural work sequential assignment is required and, due to the broad nature of the peaks in the paramagnetic forms of Dx, assignments via standard 2D experiments are impossible for these forms. To overcome the problem of line broadening by these paramagnetic centers, the

Fe can be replaced by a diamagnetic equivalent. The 1D spectrum of the Zn analogue of Dx shows all resonances sharp and within the 0–10 ppm region. Using the Zn form, sequential assignment can be carried out and standard 2D NMR techniques used to determine a solution structure.[13]

Initial spectra in D_2O for Dx(Zn) contained very slowly exchanging amide backbone protons, indicating extensive H-bonding. Subsequent identification of the spin systems was carried out using TOCSY and DQF-COSY experiments. Sequential assignment was carried out in conjunction with a NOESY spectrum.

NMR structure determination requires the complete assignment of a NOESY spectrum followed by integration of all cross peaks. These cross peaks, which contain information about through space interactions between adjacent protons in the protein under study, must be calibrated to obtain distance information. A set of distance constraints is obtained which can then be used to generate a set of structures. Various algorithms can be used and many commercial programs are available to carry out this task. For Dx(Zn) the distance geometry program DIANA was used to generate a family of structures from the NMR data. The global RMSD for the backbone residues, which is a measure of how similar the set of NMR structures are, of the NMR family was 0.63 Å. The RMSD values for each residue in the backbone actually showed variations, with structural disorder (i.e., higher RMSD values) being seen for the region Glu20–Thr25 and the N-terminus. This may actually refect flexibility in solution for these regions or may arise, for the Glu20–Thr25 region, from a lack of NOE constraints.

Comparison Between Solution and Crystal Structures
2D-NMR Versus X-Ray

X-ray and NMR results give structures with complementary information. NMR gives a family of structures which represent the solution state picture. NMR can also give information about any mobility which may be present in the protein under study. X-ray structures represent the solid state conformation. However, even though X-ray and NMR structures are determined using different states of matter, most of the protein structures thus far determined by NMR and X-ray show few differences, suggesting that the solid state conformation is a good representation of the true solution state picture.

Overall, the similarity between the structures from the NMR family and that from X-ray is good. Figure 7 shows a superposition of nine NMR structures with the 3D crystallographic structure determined for the dimer. All the structural elements seen in the X-ray structure are present in the NMR

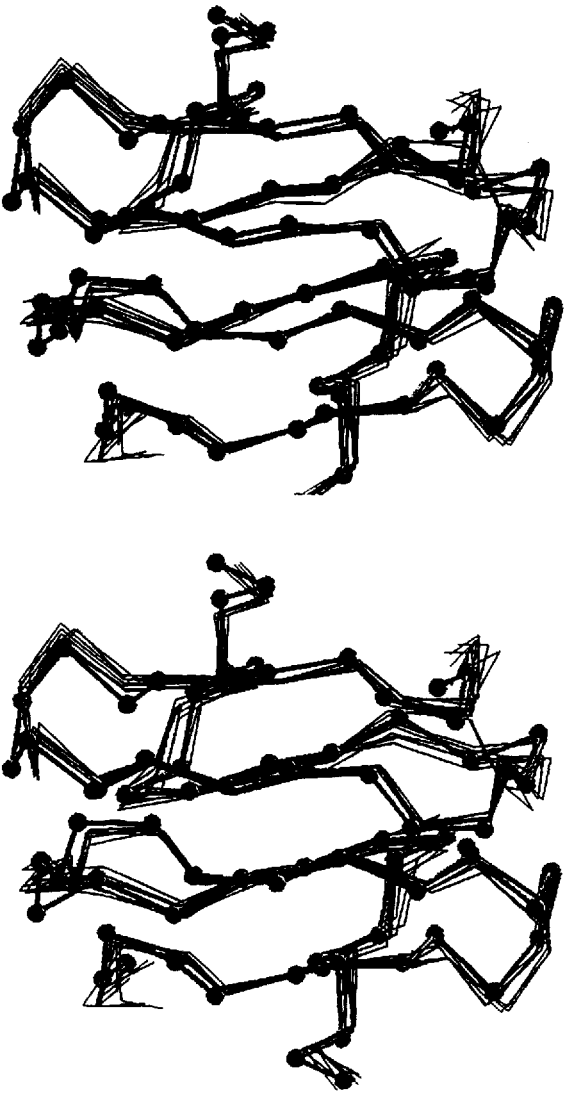

FIGURE 7 Comparison of crystal (X-ray) and solution (2D NMR) structures.

family.[7,13] The backbone RMSD between the X-ray and NMR structures is 1.33 Å. The relative positions of the monomers in the Dx dimer are very similar in both the X-ray structure and the Dx NMR. The differences observed between the NMR and X-ray structures are probably a result of a lack of NOE's rather than genuine structural differences. It can be concluded that the solution and solid state structures of Dx are very similar, and replacement of the Fe by Zn does not change the structure of the protein.

ASSOCIATION OF RUBREDOXIN TYPE CENTERS WITH OTHER METAL SITES

Several cases have been found in which Dx and Rd centers appear in association with other types of iron centers. In *Desulfoferrodoxin* (Dfx), a single polypeptide chain (14 kDa) provides the binding motif for the Dx-type center and for another mononuclear octahedral iron center with N/O ligands and possibly cysteine ligand(s). This protein probably had its origin in a gene fusion process where the 4 kDa N-terminal domain (bearing strong homology with the Dx sequence) was joined with a 10 kDa polypeptide (from a protein containing the mononuclear octahedral center).[27] Another case is *Rubrerythrin* (Rh), a dimer of 21 kDa, containing (per subunit) one Rd center and a binuclear cluster, similar to the ones found in Hemerythrin or Ribonucleotide Reductase B2 subunit.[28] Although the function of these proteins is still unknown, it is clear that both Dx and Rd type centers exist in association with other metal centers, giving multi-center proteins.

CONCLUSIONS

Structural Comparison of Desulforedoxin and Rubredoxin

Several factors have been outlined which have been postulated to play a role in the modulation of the redox properties of the iron–sulfur center: the metal plus the ligand complex, aromatic side chains, the NH–S hydrogen bonding pattern and the environment of the metal site.[2,29] With respect to the first, no great differences are found between Dx and Rd. In respect to the aromatic residues, for Dx, only one single aromatic residue is present, Tyr7, which is also present within the Rds of the *Desulfovibrio* family. In fact, in the Dx molecule, Tyr7 can be exactly superimposed on Tyr4 from the *Desulfovibrio* family of Rds. From these considerations it is not surprising that no great difference is found between the redox potential of Dx (–35 mV) and Rds (0 to –50 mV).

Dx and Rd, both small Fe–S_4 containing proteins, are structurally similar in many respects. Primary sequence comparison of Rds and Dx shows that, in spite of the folding homologies between both structures, the only conserved residues are the cysteines involved in metal binding plus a few neighboring residues (see scheme in Fig. 1). However, apart from the partial superposition of the Dx and Rd backbones, another common feature is the presence of an internal hydrophobic core,[7] which is rather aromatic in Rd structures.[2]

The β-sheet present in both the Rds and Dx can be superimposed, giving a RMSD of 1.33 Å.[7] The region after the anti-parallel β-sheet is completely different in the two proteins, mainly as a result of the dimeric nature of Dx. Rd has two loops after the end of the anti-parallel β-sheet, allowing a hydrophobic aromatic core to form. Dx has an extended conformation which runs parallel to the anti-parallel β-sheet forming a planar face. This is the region of interaction between the Dx monomers. The representation shown in Fig. 8 (color plate at the end of this article) of the Dx dimer and Rd (Cα carbons) highlights these points for both structures. The conserved β-sheets (Glu4–Val19 in Dx) plus the C-terminus strand are marked in red.

A comparison of the NH–S H-bonding pattern between Dx and Rd shows (Fig. 9, color plate at the end of this article) for Rd, 6 NH–SH bonds with lengths of around 2.6 Å. Dx has 3 NH–SH bonds and one NH–SH bond between the Nε of Gln14 and Cys28. All are around 2.8 Å. It seems that Dx has fewer and longer NH–SH bonds as a result of the geometrical constraints imposed by the adjacent cysteines.

Coordination Sphere at the Metal Site[7]

As mentioned above, the striking similarity of the main chain atoms of Dx and Rd includes the region of the cysteinyl ligands, which corresponds to the conserved pattern in Dx and Rd, X–Cys–X–X–Cys–Gly. On the other hand, the vicinal dithiol moiety, X–Cys–Cys–Gly, is different. The extra residues between cysteines 39 and 42 in Rd as compared to Dx results in differences in the Fe–S bond angles as expected. This turn, in Rd, is at roughly 90° to the anti-parallel β-sheet. In Dx, the turn is more parallel to the β-sheet, partly due to the constraints imposed by the adjacent cysteines and partly due to the presence of the other monomer. There are also sections of β-sheet at the C-termini of Dx and Rd spatially arranged in a similar manner relative to the anti-parallel β-sheet (Fig. 8).

Nevertheless, overall the Fe–S_4 geometries are globally very similar for both Dx and Rd structures, although Cys–Cβ atom positions, for vicinal cysteines, are rather displaced when comparing both structures. The differences between Dx and Rd are subtle: in Rd the coordination around the iron atom is symmetrical, with pseudo twofold symmetry. In Dx, the –X–Cys28–Cys29–X motif forces a totally different structure stabilized by different kinds of NH--S bonds and a distortion of the Sγ–Fe–Sγ bond angle. A single additional hydrogen bond occurs between main chain nitrogen atom NCys28 and side-chain oxygen atom Nε of Gln14 (Fig. 9).

The similarity found between Dx and Rd due to the conserved motiv Cys–X–X–Cys has been recently described in the literature[30] as a type of zinc-binding motif (the so-called rubredoxin "knuckle"). This type of folding around the metal, and exemplified by Schwabe and Klug for several zinc-binding proteins, is identical to the corresponding "knuckle" found in Dx.

In conclusion, the two vicinal cysteines in the Dx sequence, Cys28 and Cys29, force a unique fold of the polypeptide chain, while the Cys–X–X–Cys pattern maintains the usual observed Rd folding. As a result, the coordination of the metal in Dx has a distinct environment and lacks the pseudo-twofold symmetry found in Rd structures. Analyzing the second coordination sphere of the Dx and Rd centers highlights several structural differences. Contrary to the finding for Rd, the Dx molecule has several polar residues, as well as ordered internal water molecules.

Spectroscopy, Genetics and Mimetic Proteins

The high-resolution X-ray structure of Dx has allowed an accurate description of the global folding, dimer structure and metal site geometry, necessary for a detailed analysis of electron transfer mechanisms and the explanation of observed spectroscopic data.

The total chemical synthesis of Dx was achieved in two phases:[17] the chemical synthesis of the 36 amino acid polypeptide chain, and the incorporation of iron at the active site. Thus for Dx it is possible to completely synthesize a metalloprotein based on the knowledge of the primary sequence. In spite of the simplicity of this case, the synthetic scheme was anticipated to be of great interest for the study of these types of iron–sulfur centers. The synthesis of analogous polypeptide chains, where specific modifications are introduced, has parallels with site mutagenesis procedures. This type of approach also allows the use of model peptides to study Fe–S centers. The advantage of peptide synthe-

sis is simplicity, ease of production, and the ability to incorporate unusual groups into the polypeptide chain.

Expression in *E. coli*, coupled with the site-directed mutagenesis, has allowed the determination of the effect of the spacing between the adjacent cysteine pair at the carboxy terminus (Cys28 and Cys29).[19] Peptides with different numbers and types of intervening residues can be prepared, allowing a correlation between the geometry of the metal site and its corresponding spectroscopic properties. In particular, the effect of spacer residues on the optical (e.g., absorbance maxima and extinction coefficients) and EPR (e.g., E/D values) properties is currently being explored.[19] Future work may focus on the analysis of crystals of other metal derivatives, allowing the study of the influence of change of d-shell electrons on the structure itself and possible correlation with spectroscopic properties.

Another interesting point to be considered is the investigation of the redox and magnetic properties of $Fe–S_4$ proteins, even in cases in which these types of centers appear in connection with other metal centers. One example of this strategy would be to model the rubredoxin center in rubrerythrin. These centers have mid-point oxidation-reduction potentials significantly higher than the values normally found in rubredoxins (200 mV higher).[28] It has been assumed that this abnormal value is due to charge effects at the iron site (presence of basic amino acid residues close but not coordinated to the iron center). The use of the basic primary structure of Rd and the subsequent manipulation of specific regions, which mimic the center present in Rubrerythrin, would allow a study of the influence of the primary structure in the oxidation-reduction properties of the metal center.

EPR and High-Spin Ferric Sites

EPR spectroscopy is a sensitive probe for the detection of paramagnetic molecules in metalloproteins. It can be used to characterize the high-spin ferric ion, in low-symmetry environments, such as those found in Dx and Rd. The so-called $g = 4.3$ EPR resonance, which arises from the middle Kramers doublet, has been associated with a rhombic distortion ($E/D = 0.3$), but the actual geometry and ligand environment of the metal center is not easily discerned from an investigation of the EPR properties alone. A comparison with model systems is useful but is also open to misinterpretation. For example, Fe(III)–DPTA complexes give rise to EPR spectra with g-values corresponding to an E/D value close to that observed for Dx. This led to the erroneous hypothesis that, in addition to sulfur ligands, oxygen and/or nitrogen could also serve as ligands to the Dx cen-

ter.[31] Thus methods in addition to EPR, such as Mössbauer, NMR or X-ray methods, should be employed in order to unambiguously discern structural details of the metal center.

Final Tales from Rubredoxin and Desulforedoxin

Dx is the smallest electron transfer protein known. The active center has structural homology with the simple $Fe–S_4$ site found in Rds. However, the study of Dx brought up an interesting aspect related to the fine design, tunning and engineering of this active site, by modulation of ligand spacing in the primary structure of the protein. The data discussed in this article relate to native protein, totally chemically synthesized protein, and cloned-overexpressed protein, as well as mutants that introduce site mutagenesis with variability of the spacing between the coordinating cysteine ligands. NMR has now been explored in native and overexpressed materials and in metal derivatives (zinc and cadmium). The mutated proteins are now under current study by X-ray crystallography and 2D-NMR. Paramagnetic metal derivatives such as cobalt and nickel are of great interest. In particular, the nickel derivative will be an inspiring unit for the hydrogenase case. Related aspects, such as peptide simple chemical models, will add additional information and will be considered in parallel.

Acknowledgments

F.R. was a PRAXIS XXI visiting scientist in Portugal. This work was supported by Grants from NIH GM 46865 and Mayo Foundation (F.R.), and Junta Nacional de Investigação Cientifica e Tecnológica and Praxis (I.M. and J.M.). Discussions with several European colleagues under contract ERBCHRXCT920014 are acknowledged (J.M.).

References

1. I. Moura, P. Tavares and N. Ravi, in *Methods in Enzymology*, Vol. 243, eds. J. LeGall and H. D. Peck, Jr. (Academic Press, New York, 1994), Chap. 14, pp. 203–215.
2. L. C. Sieker and J. LeGall, in *Methods in Enzymology*, Vol. 243, eds. J. LeGall and H. D. Peck Jr. (Academic Press, New York, 1994), Chap. 15, pp. 216–241.
3. I. Moura, M. Bruschi, J. LeGall, J. J. G. Moura A. V. and Xavier, Biochem. Biophys. Res. Commun. **75**, 1037–1044 (1977).
4. I. Moura, R. Cammack, M. Bruschi and A. V. Xavier, Biochim Biophys. Acta **533**, 156–162 (1979).
5. I. Moura, B. H. Huynh, J. LeGall, A. V. Xavier and E. Munk, J. Biol. Chem. **255**, 2493–2498 (1980).

6. M. Bruschi, I. Moura, L. Sieker, J. LeGall and A. V. Xavier, Biochem. Biophys. Res. Commun. **90**, 596–605 (1979).
7. M. Archer, R. Huber, P. Tavares, I. Moura, J. J. G. Moura, M. A. Carrondo, L. C. Sieker, J. LeGall and M. J. Romão, J. Mol. Biol. **251**, 690–702 (1995).
8. I. Moura, M. Teixeira, A. V. Xavier, J. J. G. Moura, P. A. Lespinat, J. LeGall, Y. Berlier, P. Saint-Martin and G. Fauque, Rec. Trav. Chim. Pays-Bas **106**, 418 (1987).
9. Y. H. Huang, I. Moura, J. J. G. Moura, J. LeGall, J. B. Park, M. W. Adams and M. K. Johnson, Inorg. Chem. **32**, 406–412 (1993).
10. V. K. Yachandra, J. Hare, I. Moura and T. G. Spiro, J.Am. Chem. Soc **105**, 6455–6461 (1983).
11. P. R. Blake, J.-B. Park, F. O. Bryant, S. Aono, J. K. Magnuson, E. Eccleston, J. B. Howard, M. F. Summers and M. W. W. Adams, Biochemistry **30**, 10885–10895 (1991).
12. P. R. Blake, J.-B. Park, Z. H. Zhou, D. R. Hare, M. W. W. Adams and M. F. Summers, Protein Sci. **1**, 1508–1521 (1992).
13. B. J. Goodfellow, P. Tavares, M. J. Romão, M. A. Carrondo, C. Czaja, F. Rusnak, J. LeGall, I. Moura and J. J. G. Moura, J. Biol. Inorg. Chem. **1**, 341–354 (1996).
14. A. Volbeda, M. H. Charon, C. Piras, E. C. Hatchikian, M. Frey and J. C. Fontecilla-Campus, Nature **373**, 580–587 (1995).
15. P. Saint-Martin, P. A. Lespinat, G. Fauque, Y. Berlier, J. LeGall, I. Moura, M. Teixeira, A. V. Xavier and J. J. G. Moura, Proc. Natl. Acad. Sci., U.S.A. **85**, 9378–9380 (1988).
16. I, Moura, A. Macedo and J. J. G. Moura, in *Advanced EPR in Biology and Biochemistry*, ed. A. J. Hoff (Elsevier, Amsterdam, 1989), pp. 813–838.
17. P. Tavares, J. K. Wunderlich, S. G. Lloyd, J. LeGall, J. J. G. Moura and I. Moura, Biochem. Biophys. Res. Comm. **208**, 680–687 (1995).
18. C. Czaja, R. Litwiller, P. Tavares, J. LeGall, J. J. G. Moura and I. Moura, J. Biol, Chem. **270**, 20273–20277 (1995).
19. L. Yu, M. Kennedy, C. Czaja, P. Tavares, J. LeGall, J. J. G. Moura and I. Moura, J. Biol. Chem, submitted (1996).
20. B.-H. Oh and J. L. Markley, Biochemistry **29**, 3993–4004 (1990).
21. L. Banci, I. Bertini, A. Diky, D. H. Kastrau, C. Luchinat and P. Sompornpisut, Biochemisty **34**, 206–219 (1995).
22. L. Banci, I. Bertini, L. D. Eltis, I. C. Felli, D. H. Kastrau, C. Luchinat, M. Piccioli, R. Pierattelli and M. Smith, Eur. J. Biochem **225**, 715–725 (1994).
23. I. Bertini, A. Diky, D. H. Kastrau, C. Luchinat, and P. Sompornpisut, Biochemistry **34**, 9851–9858 (1995).
24. I. Bertini, A. Donaire, B. A. Feinberg, C. Luchinat and H. Yuan, Eur. J. Biochem **232**, 192–205 (1995).
25. M. T. Werth, D. M. Jr. Kurtz, I. Moura and J. LeGall, J. Am. Chem. Soc. **109**, 273–275 (1987).
26. B. Xia, W. M. Westler, H. Cheng, J. Meyer, J.-M. Moulis and J. M. Markley, J. Am. Chem. Soc. **117**, 5347–5350 (1995).
27. P. Tavares, N. Ravi, J. J. G. Moura, J. LeGall, Y. H. Huang, B. R. Crouse, M. J. Johnson, B. H. Huynh and I. Moura, J. Biol. Chem. **269**, 10504–10510 (1994).
28. J. LeGall, B. C. Pickril, I. Moura, A. V. Xavier, J. J. G. Moura and B. H. Huynh, Biochemistry, **257**, 1636–1642 (1988).
29. E. T. Adman, K. D. Watenpaugh and L. H. Jensen, Proc. Natl. Acad. Sci., U.S.A. **72**, 4854 (1975).
30. J. W. R. Schwabe and A. Klug, Structural Biology **1**, 345–349 (1994).
31. M. F. J. M. Verhagen, W. G. B. Voorhorst, J. A. Kolkman, R. B. G. Wolber and W. R. Hagen, FEBS Lett. **336**, 13–18 (1993).